The LANS-α and Leray turbulence parameterizations in primitive equation ocean modeling

2008 J. Phys. A: Math. Theor. 41 344009

(http://iopscience.iop.org/1751-8121/41/34/344009)

IOP PUBLISHING JOURNAL OF PHYSICS A: MATHEMATICAL AND THEORETICAL

J. Phys. A: Math. Theor. **41** (2008) 344009 (23pp) doi:10.1088/1751-8113/41/34/344009

The LANS-α and Leray turbulence parameterizations in primitive equation ocean modeling

M W Hecht[1], **D D Holm**[1,2], **M R Petersen**[1,3] **and B A Wingate**[1,3]

[1] Computer, Computational and Statistical Sciences Division, Los Alamos National Laboratory, Los Alamos, NM, USA
[2] Mathematics Department, Imperial College London, UK
[3] Center for Nonlinear Studies, Los Alamos National Laboratory, Los Alamos, NM, USA

E-mail: mpetersen@lanl.gov

Received 30 November 2007, in final form 28 April 2008
Published 11 August 2008
Online at stacks.iop.org/JPhysA/41/344009

Abstract

Ocean modeling presents several unique technical challenges: there is a tremendous range of spatial scales; the kinetic energy forcing scale occurs at the Rossby radius of deformation (20–100 km), which is often at or below the grid resolution; and mixing is strongly anisotropic, occurring primarily along nearly horizontal isopycnal surfaces. We present analysis and numerical results to show that the Lagrangian-averaged Navier–Stokes alpha (LANS-α) turbulence parameterization and, to a lesser extent, the Leray parameterization are well suited to ocean modeling. LANS-α and Leray are fundamentally different from purely dissipative turbulence models in that both LANS-α and Leray are more energetic and produce more eddy structure near the gridscale. This is consistent with expectation from linear stability analysis, where it has been shown that these models resolve the process of baroclinic instability on coarser meshes than standard Navier–Stokes. Formulations of LANS-α and Leray models for the primitive equations are presented. In an idealized ocean channel domain, LANS-α produces turbulence statistics in kinetic energy, eddy kinetic energy and temperature distributions that resemble a doubled-resolution simulation without LANS-α. Leray produces qualitatively similar results, but to a lesser degree than LANS-α. Finally, the Leray model is tested in a North Atlantic domain with realistic topography and forcing, and produces higher kinetic and eddy kinetic energy than the non-Leray model.

PACS numbers: 92.10.Lq, 47.27.−i

1. Introduction

The characteristic features of turbulence—its distribution of eddy sizes, shapes, speeds, vorticity, circulation and viscous dissipation—may all be captured by using the exact

Navier–Stokes equations. These equations correctly predict how the cascade of turbulent kinetic energy and vorticity accelerates and how turbulence stretches itself into finer and finer 'sinews' of vorticity, until its motion reaches only a few molecular mean free paths and it may finally be dissipated by viscosity into heat. However, the accuracy of the Navier–Stokes equations in capturing the cascade of turbulent kinetic energy into finer and finer scales by vortex stretching is also the cause of serious problems in direct numerical simulations of turbulence.

Landau estimated that the number of active degrees of freedom required to simulate the turbulent cascade increases with Reynolds number as $Re^{9/4}$ [1], which is the ratio of the domain size to the Kolmogorov dissipation length. This geometric rate of increase in resolution requirements as a function of Reynolds number would quickly outstrip the numerical resolution capabilities of even the largest computer (see, e.g., [2] section 7.4). Therefore, to make turbulence computable, scientists must rely on approximate models that slow the cascade into smaller, faster eddies. In most numerical models, this effect is accomplished by artificially increasing the viscosity, which causes the eddies below a certain size to dissipate computationally into heat. This dissipative imperative causes errors in numerical simulations, though, because it damps out the variability (known as intermittency) in the larger-scale flow. Flow variability is caused by the myriad of small scales of motion interacting nonlinearly together while being swept along by the larger motions. Thus, computational turbulence closure models based on enhancing viscous dissipation over its physical Navier–Stokes value run the risk of producing unrealistically low variability.

Perhaps surprisingly, one of the first clues in understanding how to develop numerical models for computing turbulence without enhancing viscous dissipation came from the great mathematical analyst Leray [3] who showed how to regularize the Navier–Stokes equations by modifying their nonlinearity to the well-known form

$$\frac{\partial \mathbf{v}}{\partial t} + \mathbf{u} \cdot \nabla \mathbf{v} + \nabla p = \nu \Delta \mathbf{v} + \boldsymbol{f}(\mathbf{x}), \quad \operatorname{div} \mathbf{u} = 0, \tag{1}$$

with $\mathbf{v} = 0$ on the boundary. Here ν is the (constant) kinematic viscosity coefficient, $\boldsymbol{f}(\mathbf{x})$ is the prescribed external force and

$$\mathbf{u} = G_\alpha * \mathbf{v} \tag{2}$$

is a filtered version of the regularized velocity $\mathbf{v}$. The filtering operation is defined by

$$G_\alpha * \mathbf{v} = \int G_\alpha(\mathbf{x}, \mathbf{y}) \mathbf{v}(\mathbf{y}) \, \mathrm{d}^3 y \tag{3}$$

for a symmetric kernel $G_\alpha(\mathbf{x}, \mathbf{y})$ of characteristic width α, which is usually taken to be a constant. The Navier–Stokes equations for $\mathbf{v}$ are recovered in the limit as $\alpha \to 0$, so that $\mathbf{u} \to \mathbf{v}$. Leray's equations (1) are said to regularize the Navier–Stokes equations, because Leray was able to prove that the modified equations (1) possess strong unique solutions that converge (in a certain weak sense) to Navier–Stokes solutions in the limit as $\alpha \to 0$. Existence and uniqueness of Navier–Stokes solutions is one of the famous $1M Clay Prize problems. For a review of the Leray regularization of the Navier–Stokes equations, see Gallavotti [4].

One of the points made by Gallavotti in [4] is that Leray's regularization of the Navier–Stokes equations no longer satisfies the Kelvin circulation theorem, since for the Leray equations (1)

$$\frac{\mathrm{d}}{\mathrm{d}t} \oint_{c(\mathbf{u})} \mathbf{v} \cdot \mathrm{d}\mathbf{x} = \oint_{c(\mathbf{u})} \left(\frac{\partial \mathbf{v}}{\partial t} + \mathbf{u} \cdot \nabla \mathbf{v} + \nabla \mathbf{u}^T \cdot \mathbf{v} \right) \cdot \mathrm{d}\mathbf{x} \neq \oint_{c(\mathbf{u})} (\nu \Delta \mathbf{v} + \boldsymbol{f}) \cdot \mathrm{d}\mathbf{x}. \tag{4}$$

in which the integration is performed around a closed fluid loop $c(\mathbf{u})$ moving with the particle velocity $\mathbf{u}$.

Remarkably, combining the process of Lagrangian averaging with Taylor's hypothesis (that sufficiently small fluctuations are swept along by the larger scales of the mean flow) leads to a regularized set of equations that answer the challenge of [4] to produce a regularization of the Navier–Stokes equations which does possess a Kelvin circulation theorem. These regularized equations comprise the LANS-α model [5],

$$\frac{\partial \mathbf{v}}{\partial t} + \mathbf{u} \cdot \nabla \mathbf{v} + \nabla \mathbf{u}^T \cdot \mathbf{v} + \nabla p = \nu \Delta \mathbf{v} + \boldsymbol{f}(\mathbf{x}), \quad \text{div } \mathbf{u} = 0. \tag{5}$$

In the LANS-α model, the filtering relation $\mathbf{u} = G_\alpha * \mathbf{v}$ for the advection velocity in the LANS-α model is specified for a constant value of α as

$$\mathbf{v} \equiv \mathbf{u} - \alpha^2 \Delta \mathbf{u}, \tag{6}$$

so that one also has div$\mathbf{v} = 0$. One immediately sees that the LANS-α model satisfies the Kelvin circulation theorem, since integration of (5) around a Lagrangian loop $c(\mathbf{u})$ implies

$$\frac{\mathrm{d}}{\mathrm{d}t} \oint_{c(\mathbf{u})} \mathbf{v} \cdot \mathrm{d}\mathbf{x} = \oint_{c(\mathbf{u})} (\nu \Delta \mathbf{v} + \boldsymbol{f}) \cdot \mathrm{d}\mathbf{x}. \tag{7}$$

The Coriolis force required for simulations of rotating fluids naturally fits together with the LANS-α model. Indeed the algorithm for expressing the LANS-α model in a rotating frame may be written simply as

$$\frac{\mathrm{d}}{\mathrm{d}t} \oint_{c(\mathbf{u})} (\mathbf{v} + \mathbf{R}) \cdot \mathrm{d}\mathbf{x} = \oint_{c(\mathbf{u})} (\nu \Delta \mathbf{v} + \boldsymbol{f}), \tag{8}$$

where $\nabla \times \mathbf{R} = 2\Omega$ is the Coriolis parameter. As expected from the viewpoint of Leray regularization, one of the velocities ($\mathbf{u}$) in equation (6) is smoother than the other one ($\mathbf{v}$) by the inversion of the Helmholtz operator. The difference arises in the derivation of the LANS-α model, because the smoother velocity $\mathbf{u}$ represents only the Lagrangian mean velocity, while the rougher one $\mathbf{v}$ also contains the Lagrangian mean effects of the smaller faster fluctuations on the momentum in Newton's law of motion.

This paper will review recent progress in implementing the LANS-α and Leray models in primitive equation ocean-climate models. To set the stage, we describe the effects of mesoscale eddies in the ocean in section 2, and compare LANS-α to current parameterizations of mixing processes. In section 3, we discuss the effects of LANS-α on ocean dynamics, in particular the Rossby radius of deformation and baroclinic instability. The model equations and numerical implementation are summarized in section 4, and in section 5 we present results from an idealized ocean channel domain and a realistic North Atlantic domain. Conclusions are presented in section 6.

2. Parameterization of mesoscale eddies

The oceans present an extremely challenging range of scales. In spatial terms, they span the globe, and yet the first internal Rossby radius, discussed in section 3, presents a much smaller length at which mesoscale turbulence occurs than that found in the atmosphere. In the temporal realm, we must consider processes driven by the diurnal cycle while allowing for the millennial scale equilibration of deep and intermediate waters.

Processes of mixing underlie these extreme scales, and the difficulty of resolving the vast range of scales raises our interest in turbulence modeling. The oceanic mixing processes we address in general circulation models can be understood in terms of four classes of mixing: (1) mixing associated with mesoscale eddies; (2) the ubiquitous mixing driven by microscopic processes and the smallest turbulent scales; (3) mixing associated with breaking internal

waves; and (4) strong vertical mixing due to convective instability, which leads to deep water formation at high latitudes.

LANS-α is primarily concerned with parameterizing the effects of mesoscale eddies. LANS-α should not be confused with mixing parameterizations that compute artificially large vertical diffusion coefficients to compensate for the sub-grid scale effects of (3) and (4), such as KPP [6] or Pacanowski and Philander [7]. LANS-α parameterizes horizontal mesoscale effects, and so may be run in conjunction with these schemes. Unlike most turbulence parameterizations, LANS-α does not add diffusivity; it modifies the nonlinear terms and can produce higher and more realistic levels of horizontal eddy kinetic energy.

Mesoscale eddies are responsible for mixing, and yet they can be understood as giving rise to that mixing through a process of stirring. While mixing is irreversible and stirring is, in theory, reversible, a more tangible characteristic of stirring is the development of structures which feed back on the dynamics. In the case of stirring by eddies, the principal structure of the eddy is strongly geostrophic, with the balance of forces dominated by pressure gradient and Coriolis terms. Effects of mesoscale eddies include the transport of heat and kinetic energy, feedback of turbulence onto the placement of large-scale structures like western boundary currents, and the flattening of isopycnals through baroclinic instability.

A widely used parameterization of mesoscale eddies is Gent–McWilliams (GM), which mimics scalar mixing in two ways: it rotates horizontal diffusivity to act along isopycnals and diffuses the layer thickness contained between isopycnals [8–11]. Global simulations with GM have a poleward heat flux that is closer to observations, so that no surface heat flux corrections are required [12]. This was a major accomplishment and GM is now a standard parameterization in climate change simulations. However, major aspects of eddy parameterization remain to be addressed. GM has been shown to present an unrealistically high sensitivity of Southern Ocean circumpolar transport to changes in the amplitude of wind forcing [13]. Model simulation of the correct path of the Gulf Stream and North Atlantic current system has also defied efforts at parameterization, apparently requiring explicit resolution of mesoscale eddies [14].

LANS-α and GM both aim to parameterize the effects of mesoscale eddies, but are very different in their implementation. GM changes the *tracer* equations (salinity, temperature) and mimics the action of eddies by flattening the density surfaces. LANS-α primarily changes the *momentum* equation, and allows more eddies to exist near the gridscale. Thus GM and LANS-α may be run in the same simulation without conflict.

Ocean models produce a spectrum of eddies which compare favorably, at least through their surface expression, with analysis of satellite-born altimetry when the model is configured at a resolution of around $1/10^\circ$ in latitude and longitude [14]. It is clear that our simulations have not converged, in a numerical sense, even at such a computationally demanding spatial resolution, as shown in the physically simplified configuration of [15].

The role of parameterization of horizontal mixing is much reduced at these more strongly eddying resolutions. Many simulations rely on just hyperviscosity and hyperdiffusivity, of a biharmonic or fourth-order form, for noise control (see, for instance, [16]). Others have found either a need to also include a Laplacian term [17], or else have argued that there may be some benefit yet to including the more physically based and less-scale selective dissipation operator [18, 19].

Even as our reliance on parameterizations of mixing is reduced at ocean model resolutions on the order of $1/10^\circ$, the sensitivity to parameterization remains high [20]. The computational cost of explicitly including a strong mesoscale eddy field at these very high resolutions is such that only very short and as yet unpublished pilot simulations, of no more than 10 years,

have been performed within a fully coupled climate system, following ocean-only global simulations of a few decades length [16, 21].

In regional ocean models, spanning only an ocean basin, it will be possible in the near future to run at the resolutions found to be convergent by [15]. However, one should expect sub-mesoscale processes, absent from their simpler model configuration, to remain only partially resolved. Even if these sub-mesoscale effects are ignored, we can expect the rapid rise of computing cost with resolution to ensure that we are working within this not-yet-converged regime for at least another decade.

Our interest in the LANS-α turbulence model for oceanography and climate science lies in the possibility of achieving the statistics of a high-resolution ocean circulation model, which includes the effect of mesoscale eddies, but at substantially lower computational cost than that dictated by use of $1/10^\circ$ resolution.

We have argued that the LANS-α model is fundamentally different from other schemes: the schemes currently in use in ocean models are primarily dissipative, whether based on the simplest isotropic and spatially invariant form or a more sophisticated form, such as that based on the work of Smagorinsky [22, 23]. In contrast, the LANS-α model's primary mechanism for accounting for the effects of the small scales on the large is fundamentally nondissipative. We proceed to discuss the effect of the use of LANS-α from an oceanographic perspective, before going on to describe the incorporation of this very different turbulence parameterization in the primitive equations of an ocean general circulation model.

3. Effects of LANS-α on ocean modeling

In this section, we first discuss some differences between realistic ocean modeling and idealized models to motivate the second part of the discussion—the effect of models on the *pathways* to turbulence via fluid dynamical instabilities.

In realistic ocean models not only are there complex cascades in different regions of the ocean but there are fluid instability processes, such as baroclinic and barotropic instability, that perform important conversions between kinetic and potential energy and their mean and fluctuating counterparts. These instability processes are sometimes referred to as the pathways to turbulence because they are the mechanisms that generate eddies and turbulence. For example, in wide, mid-latitude currents the baroclinic instability process dominates the dynamics by converting potential to kinetic energy [24]. The important length scale required for capturing baroclinic instability is the Rossby deformation radius.

Numerous authors, for example [24–30], discuss the role of the Rossby deformation radius in the transfer of kinetic energy, potential energy and potential enstrophy. While theories differ, it is clear that the deformation radius is a critical length scale where processes like barotropization occur (the tendency for flow throughout the depth of the ocean to couple, becoming more vertically uniform). Salmon [25], using a two-layer model, proposed a theory based on total energy and potential enstrophy transfer. At scales larger than L_R there is a forward cascade of total energy in the baroclinic mode from the forcing scale to the deformation radius. At L_R barotropization occurs and there is a net inverse cascade of the barotropic mode kinetic energy away from the deformation radius toward large scales.

Therefore, predicting the large-scale variability in the ocean requires having enough grid points to adequately resolve the Rossby deformation radius. A typical distribution of grid points in today's ocean models is shown in figure 1. It shows the zonally averaged first baroclinic Rossby radius from a 0.1° model's time-mean density along with the grid spacing for model resolutions from 0.1° to 0.8°. At the time of writing, the first 0.1° global coupled

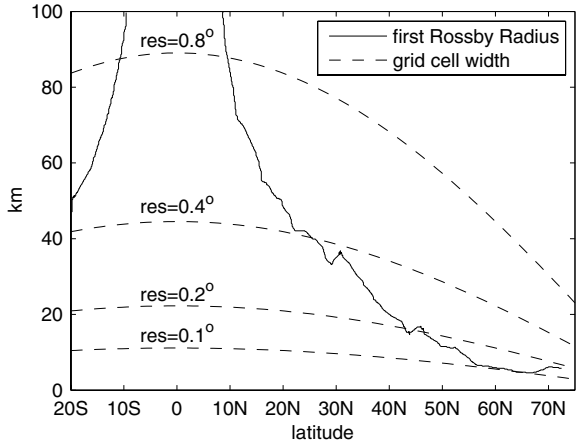

Figure 1. The solid line shows the first internal Rossby radius, zonally averaged, as diagnosed from a 0.1° North Atlantic simulation [14]. The lowest dashed line shows the model grid spacing from that 0.1° simulation, with the latitudinal dependence reflecting the convergence of the meridional grid lines which define the grid. The other three dashed lines display grid spacing for lower resolution versions of the same model grid. Only the highest resolution, 0.1° grid, maintains a spacing less than the Rossby radius at middle latitudes.

model has been run for simulation times of 10 years or less. For global climate simulations, whose resolution is often 1°, the models need to be run for centuries.

This means that one of the fundamental problems faced in contemporary ocean modeling is that there are not enough resources to adequately resolve the kinetic energy forcing scale due to fluid instability processes. Indeed, one of the successes of the GM parameterization mentioned in section 2 is that it mimics aspects of the energy conversion due to baroclinic instability.

As an example of the consequences of not including the effects of mesoscale eddies see [31, 32]. The authors show that without resolving the mesoscale eddies the depth of the thermocline, crucial to long-term climate predictions, cannot be correctly predicted.

In the remainder of this section we investigate how the LANS-α model and simple diffusion models affect the critical wavenumber for the two-layer baroclinic instability problem. In [33], for example, it was shown that the critical wavenumber for baroclinic instability to occur shifts to a lower wavenumber as a function of the modeling parameter for both eddy viscosity and the LANS-α model. For dissipation the modeling parameter is the eddy viscosity, for the LANS-α model and Leray it is the length scale, α. In both cases the effects of accounting for the small scales on the large through averaging produces neutral curves for the new, averaged variables. For both eddy viscosity and LANS-α the models produce critical wavenumbers which are lower than the unmodeled equations which indicates that baroclinic instability, and therefore the conversion of potential to kinetic energy, occurs at larger length scales, making this process more resolvable on the coarse meshes we have available today.

Though both LANS-α and eddy viscosity models lower the critical wavenumber for the onset of instability there are important differences between the two methods. In figure 2, we compare the neutral curves for constant LANS-α and constant eddy viscosity when the model equations are closed by both Laplacian dissipation and hyperviscosity ($-\nabla^4$, also called biharmonic viscosity). Figure 2(b) is a plot of the strength of the shear, relative to the β parameter, as a function of nondimensional wavenumber. Here $\beta = \mathrm{d}f/\mathrm{d}y$ is the meridional

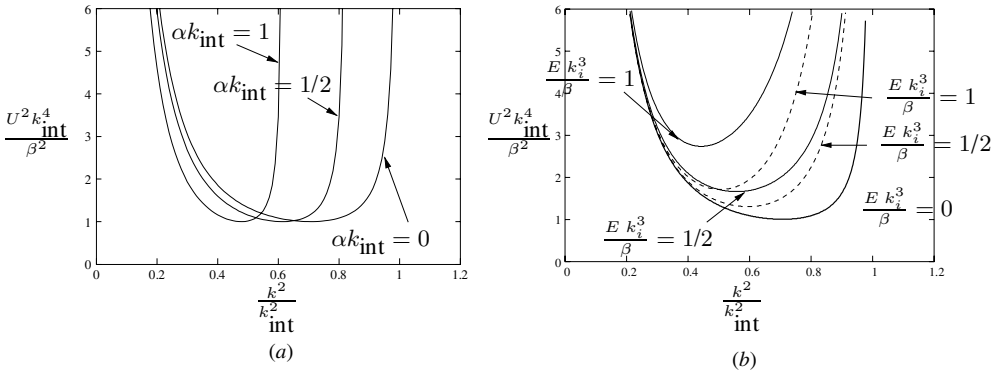

Figure 2. Neutral curves for (*a*) LANS-α and (*b*) Laplacian viscosity (solid line) and hyperviscosity (dashed line). The vertical axes are a normalized forcing strength in baroclinic instability, the horizontal axes are normalized wavenumber and areas above each curve are linearly unstable (see details in [45]). As the α parameter is increased in LANS-α (*a*) the neutral curve moves to smaller wavenumber but the minimum forcing remains constant, showing that baroclinic instability can be induced on courser grids with LANS-α. As the eddy viscosity E is increased (*b*) the minimum forcing increases, so that baroclinic instability is more difficult to induce.

derivative of the Coriolis parameter. The thick solid black line shows the neutral curve for the instantaneous equations (equations that have not been Eulerian or Lagrangian averaged). The dashed lines show how Eulerian averaged equations closed using hyperviscosity change the neutral curve for two values of the eddy viscosity, the solid lines show the same but for Laplacian dissipation. Both Laplacian diffusion and hyperviscosity shift the critical wavenumber to a lower value but *require higher forcing* to trigger instability since both rely on damping to close the equations. Figure 2(*a*) shows a plot similar to figure 2(*b*) except the model equations are Lagrangian averaged and the modeling parameter is a nondimensional measure of α. Here, increasing α again moves the critical wavenumber to a lower value but instability is triggered at the same physical forcing value as in the unaveraged case. This is an essential point that one can produce a model of averaged equations which enters a dynamically unstable regime at a realistic level of forcing, using LANS-α, at a resolution that would otherwise prove inadequate. Because this analysis is conducted on the linearized equations, all of these comments apply to the Leray model as well.

In summary, most climate models today run with grids that cannot resolve the deformation radius. Since LANS-α has the effect of moving the critical wavenumber for the onset of instability to a lower wavenumber, physics that occurs near the Rossby radius, like eddy activity and the kinetic energy forcing due to baroclinic instability, may occur in lower resolution simulations when using LANS-α than without LANS-α. Numerical simulations of both LANS-α and Leray bear out this prediction of the linear analysis; low-resolution simulations contain higher eddy activity with the turbulence parameterizations than without (see results in section 5). It would be interesting to study the effect of LANS-α on important regimes at subdeformation radius scales, but at present that is the domain of idealized models where there is adequate resolution at wavenumbers higher than the deformation radius.

4. Model implementation

In this section, we review recent progress in implementing the LANS-α turbulence parameterization in the POP primitive equation ocean model. Previous experience in

simpler geophysical fluid settings motivated the use of LANS-α in full ocean-climate models. Typically, a low-resolution experiment with LANS-α produces structures, energy spectra, and turbulence statistics that are similar to a high-resolution control simulation without LANS-α. This was true for potential and kinetic energy spectra in shallow water simulations [34] and eddy structures in a barotropic vorticity double-gyre problem [35].

The alpha version of the primitive equations are

$$\frac{\mathrm{d}\mathbf{v}}{\mathrm{d}t} - \alpha^2 \nabla^2 u_j \nabla u_j + \mathbf{f} \times \mathbf{u} = -\frac{1}{\rho_0} \nabla \pi + \mathcal{F}(\mathbf{v}), \tag{9}$$

$$\frac{\mathrm{d}\varphi}{\mathrm{d}t} = \mathcal{D}(\varphi), \tag{10}$$

$$\frac{\mathrm{d}}{\mathrm{d}t} \equiv \left(\frac{\partial}{\partial t} + \mathbf{u} \cdot \nabla + u_3 \partial_z \mathbf{v} \right) \tag{11}$$

$$\frac{\partial \pi}{\partial z} - \rho_0 \alpha^2 \nabla^2 u_j \partial_z u_j = -\rho g, \tag{12}$$

$$\pi = p - \rho_0 \frac{\alpha^2}{2} |\nabla \mathbf{u}|^2 \tag{13}$$

$$\nabla \cdot \mathbf{u} + \partial_z u_3 = 0, \tag{14}$$

$$\mathbf{u} = (1 - \alpha^2 \nabla^2)^{-1} \mathbf{v}, \tag{15}$$

where $(v_1, v_2, v_3) = (\mathbf{v}, v_3)$ and $(u_1, u_2, u_3) = (\mathbf{u}, u_3)$ are the rough and smooth velocities, ∇ is the horizontal gradient, φ is a tracer (temperature, salinity or a passive tracer), ρ is the full density, ρ_0 is the background density, p is pressure, π is a modified pressure, $\mathcal{F}$ and $\mathcal{D}$ are momentum and tracer diffusion terms, $\mathbf{f}$ is the Coriolis parameter, g is the gravitational acceleration and α is the alpha model's smoothing length scale. The primitive equations are hydrostatic (12), incompressible (14) and Boussinesq.

Many readers may be more familiar with the equivalent form of LANS-α where the line element stretching term in (9) is $v_j \nabla u_j$ rather than $-\alpha^2 \nabla^2 u_j \nabla u_j$ (to convert between forms, use (15) and absorb the extra term into the definition of π). We prefer the form shown here, as it is clear that as $\alpha \to 0$ the equation set reverts back to the standard primitive equations. The second term in (12) is the vertical component of $-\alpha^2 \nabla^2 u_j \nabla u_j$, and was not included in the current numerical implementation. As explained in [36], π is then the hydrostatic pressure in (12), and is subsequently used in the equation of state.

The LANS-α and Leray parameterizations have been implemented in the POP primitive-equation ocean-climate model. The POP model, developed and maintained at Los Alamos National Laboratory, is the ocean component of the Community Climate System Model, and is used in simulations for consensus documents of anthropogenic climate change by the Intergovernmental Panel on Climate Change [37–39]. Ocean models present a particular challenge to the implementation of LANS-α because they typically use a split barotropic/baroclinic timestepping scheme in order to reduce the computational penalty of short timesteps required by fast surface gravity waves. POP takes an implicit timestep in the barotropic (vertically integrated) mode, and explicit timesteps for the remaining baroclinic modes. An initial algorithm, derived using the primitive LANS-α equation set, proved to be too inefficient to be a useful turbulence model. However, a reduced algorithm, where one smoothing step was eliminated in the iterative implicit solve, was much faster and produced similar results [36]. The POP model with this reduced algorithm for LANS-α, referred to as POP-α, is used in this study.

A second implementation issue is how to go about smoothing the velocity in an efficient way. The smoothing operator is usually presented as a Helmholtz inversion, as in (15), but local filters have been shown to have the same effects and are much cheaper [40, 41]. In the Helmholtz inversion, the alpha parameter controls the smoothing, and thus the overall strength of the turbulence model. The equivalent in terms of the filter is the filter width and its associated weights. Due to a pressure–velocity feedback in the barotropic mode, filter weights cannot be increased arbitrarily; rather, the stencil must be made wider for stronger smoothing [41]. In the simulations presented here, filter sizes are varied from 3×3 to 9×9, and are labeled in plots by F3 to F9.

The primitive-equation Leray model retains the smoothed advecting velocity but drops the line element stretching term, so that (9) and (12) are

$$\frac{\mathrm{d}\mathbf{v}}{\mathrm{d}t} + \mathbf{f} \times \mathbf{u} = -\frac{1}{\rho_0}\nabla\pi + \mathcal{F}(\mathbf{v}), \tag{16}$$

$$\frac{\partial\pi}{\partial z} = -\rho g. \tag{17}$$

The Leray model lacks a Kelvin circulation theorem and potential vorticity conservation, both of which are possessed by the continuous, inviscid form of the LANS-α model. The POP ocean model has been implemented with both LANS-α and Leray models. The method of computation is identical except for the inclusion of the line element stretching term.

5. Results

In this section, we compare LANS-α to the Leray model in an idealized channel domain, and then describe simulations in a realistic North Atlantic domain. The LANS-α model can produce turbulence statistics in POP that resemble those from a doubled-resolution standard POP model. Instantaneous velocity fields show that POP-α actually contains stronger and more numerous eddies than POP at the same resolution (figure 3). This is borne out in globally averaged statistics: POP-α has higher kinetic energy (KE) and eddy kinetic energy (EKE, defined below) than POP, and both increase as either α (for the Helmholtz inversion) or the filter width is increased (figures 4 and 5).

It is important to realize that in ocean modeling, increasing the EKE is not a goal in itself. Rather, it is the *effect* of increased eddy activity, including transport of heat and salinity, that are critical. The statistics in figures 3–9 were produced in an idealized channel configuration that was specifically designed to invoke baroclinic instability and test the effects of eddies on the vertical temperature profile. This configuration imitates the physical forcing of the Antarctic Circumpolar Current: it includes westerly surface wind forcing and surface thermal forcing that is warm (cool) in the north (south). This produces tilted isotherms in the north–south direction, which is an unstable configuration and a source of available potential energy [31, 32]. In the real ocean, eddies transport heat and flatten the isotherms in this situation, converting the potential energy of the tilted isotherms to the KE of the eddies themselves (this is the classic description of baroclinic instability). In ocean models this process only occurs if eddies are present in the flow; thus, the vertical temperature profile is an additional diagnostic of eddy activity, and confirms whether the turbulence model achieves the proper effect on the tracers. This can be seen in the POP runs of successively doubled resolution in figure 6: at low resolution (0.8°) the isotherms are steeply inclined, resulting in warmer water at depth; at high resolution (0.1°) the same isotherm is shallow and flatter, and the deep water is colder. The increased eddy activity in POP-α results in temperature profiles that are close to

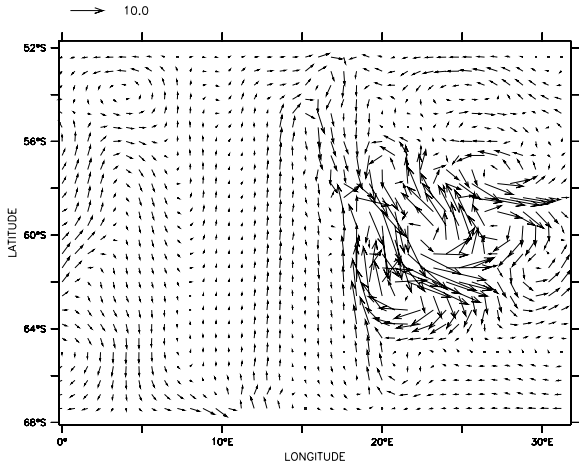

(*a*) POP, 0.4° resolution

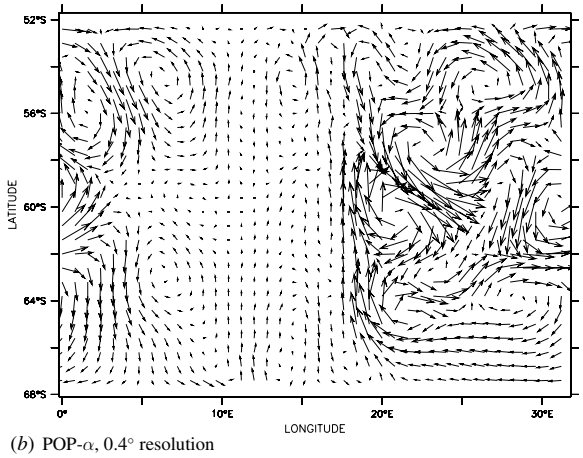

(*b*) POP-α, 0.4° resolution

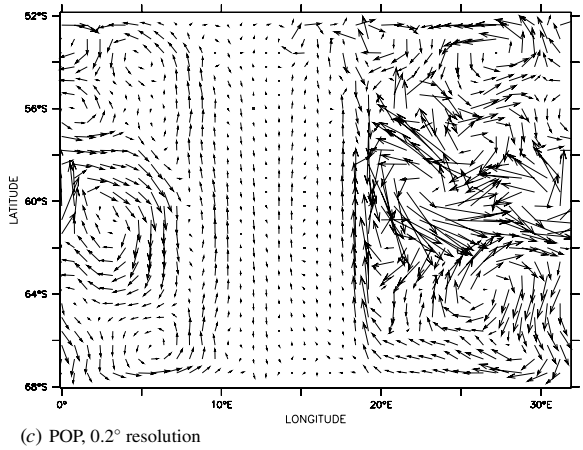

(*c*) POP, 0.2° resolution

Figure 3. Instantaneous velocity fields for POP and POP-α in the channel domain at a depth of 1626 m. Eddy activity with POP-α (*b*) is more similar to that of POP with doubled resolution (*c*). The POP-α simulation (*b*) uses a filter of width nine, and the smooth velocity field **u** is shown. All three plots use the same vector scaling.

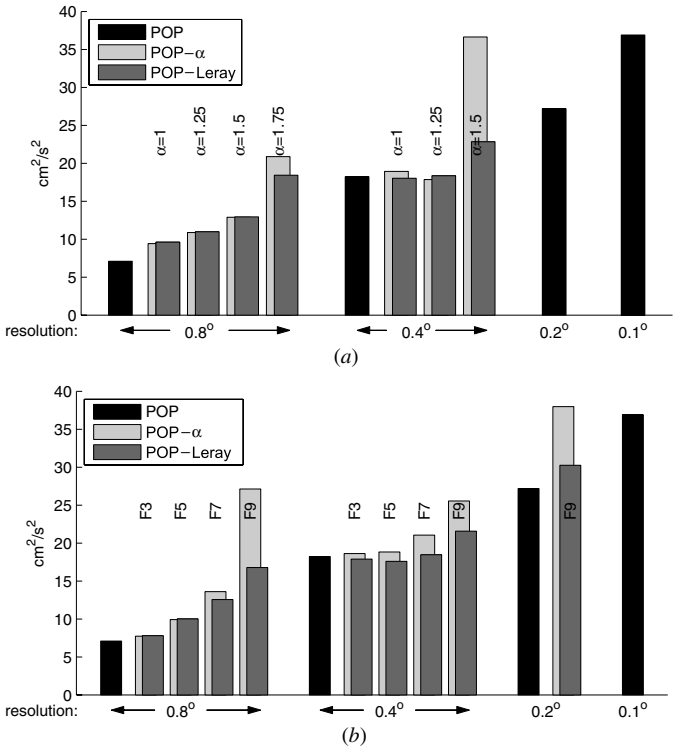

Figure 4. Globally averaged horizontal kinetic energy for all channel domain simulations, using $u_i^2/2$ for POP and $u_i v_i/2$ for POP-α and POP-Leray (see definitions in the main text). As the resolution increases with standard POP, the kinetic energy increases. Kinetic energy also increases using POP-α at fixed resolution, when either α is increased using the Helmholtz inversion (*a*) or the stencil width of the filter is increased (*b*). At the largest values of α and widest stencil (F9), the kinetic energy in POP-α is close to that of standard POP with a doubled resolution. Each value was calculated by averaging over the entire domain, and in time after 100 years for the whole simulation. Labels F3, F5 indicate a filter of width three, five, etc. In summary, POP-α can attain kinetic energy values that are similar to a doubled-resolution POP simulation using either the Helmholtz or filter smoothing method. (*a*) Kinetic energy, smoothing using Helmholtz inversion and (*b*) kinetic energy, smoothing using filters.

the POP doubled-resolution simulations. Further details of the channel domain configuration and simulations are presented in [36, 41].

Figure 7 compares the horizontal KE and EKE of POP-α and POP-Leray for 0.2° resolution simulations. There are three possible ways to measure these values:

$$\begin{aligned} \mathrm{KE}_{u^2} &= \left(u_1^2 + u_2^2\right)/2, & \mathrm{EKE}_{u^2} &= \left(\overline{(u_1')^2} + \overline{(u_2')^2}\right)/2, \\ \mathrm{KE}_{uv} &= (u_1 v_1 + u_2 v_2)/2 & \mathrm{EKE}_{uv} &= \left(\overline{u_1' v_1'} + \overline{u_2' v_2'}\right)/2, \\ \mathrm{KE}_{v^2} &= \left(v_1^2 + v_2^2\right)/2, & \mathrm{EKE}_{v^2} &= \left(\overline{(v_1')^2} + \overline{(v_2')^2}\right)/2, \end{aligned} \tag{18}$$

where u_i and v_i are the components of the smooth and rough velocities, and the prime indicates the residual from a 5 year mean. Note that KE_{uv} is the conserved quantity for the inviscid LANS-α equation [5], while KE_{v^2} is the conserved quantity for the inviscid Leray model. KE and EKE in these three norms are all larger for POP-α than for POP-Leray. However, when one compares the conserved quantity for each model, values are nearly the same. In both

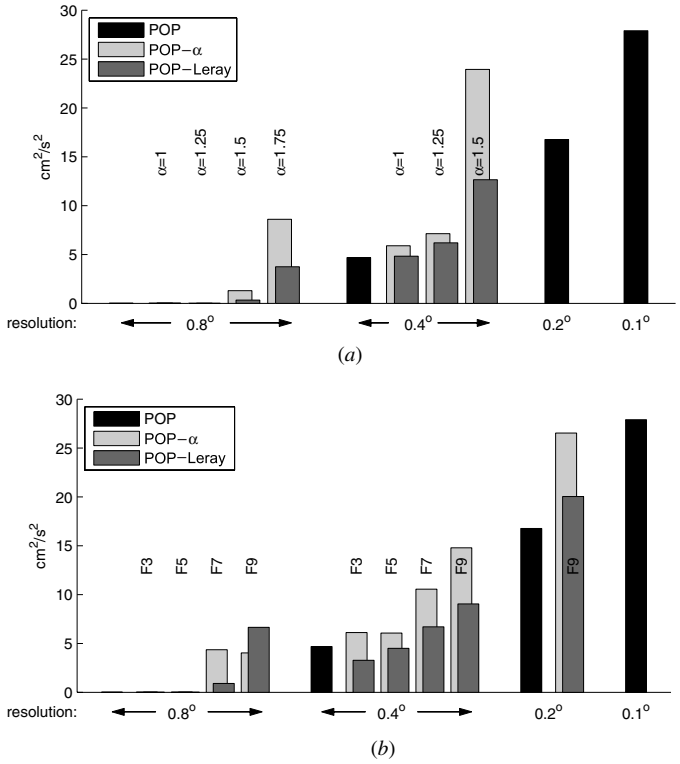

Figure 5. Same as figure 4 but for mean global horizontal eddy kinetic energy, measured as $\overline{(u_i')^2}/2$ for POP and $\overline{u_i' v_i'}/2$ for both POP-α and POP-Leray, where the bar indicates a 5 year mean and the prime is the residual. As with kinetic energy, eddy kinetic energy increases with increasing α (*a*) or filter width (*b*), so that POP-α can have eddy kinetic energy comparable to that of standard POP at doubled resolution. POP-Leray shows similar trends, but with weaker energies. Note that at the lowest resolution (0.8°) the eddy kinetic energy of standard POP is indistinguishable from zero on this scale. In summary, POP-α simulations have more eddy activity than POP simulations at the same resolution. (*a*) Eddy kinetic energy, smoothing using Helmholtz inversion and (*b*) eddy kinetic energy, smoothing using filters.

models, the flow becomes more energetic as the strength of smoothing is increased, and Leray is nearly always less energetic when measured in the same norm (figures 4 and 5). A fairer measure for comparison is the effect on the temperature, as this avoids the issue of choosing which norm to use. In all cases, POP-Leray produces temperature profiles that tend toward the higher resolution POP profiles, but POP-α performs much better (figure 6). This is similar to results from a barotropic vorticity double gyre problem, where Leray was qualitatively the same as LANS-α, but quantitatively inferior [35]. Comparisons in large eddy simulations were mixed, where Leray was better at course resolution when compared to direct numerical simulations, but LANS-α was better in a number of quantities in more fully resolved cases [40, 42].

The effects of the Helmholtz inversion versus the filter may be conveniently compared in figures 4 and 5. Both KE and EKE increase as the smoothing parameter is increased, where the smoothing parameter is α for the Helmholtz inversion or the filter width for filtering.

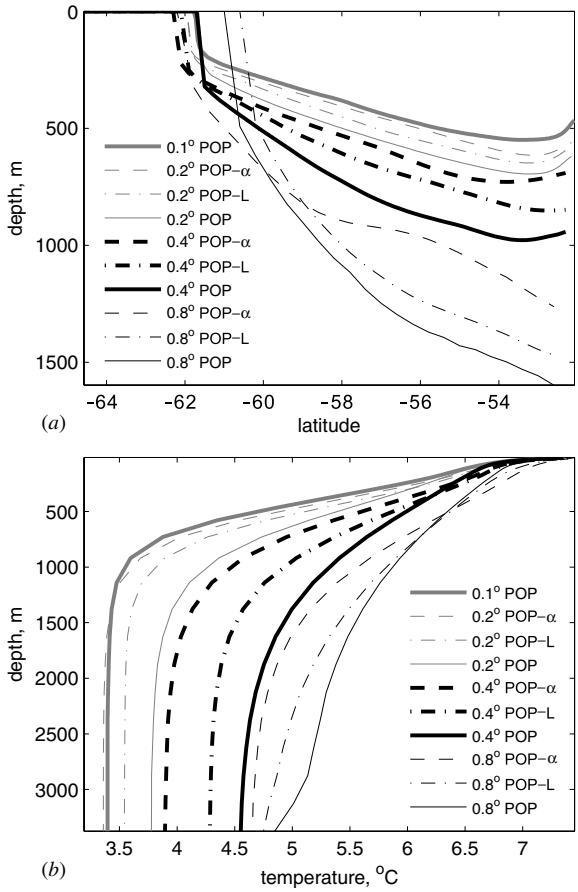

Figure 6. Comparison of equilibrium temperature distributions in the channel domain using POP, POP-α and POP-Leray, showing: (*a*) depth of 6° C isotherm of potential temperature and (*b*) horizontally averaged potential temperature versus depth. At each resolution, the curve for POP-α is comparable to that of the doubled-resolution POP case. This shows that POP-α is correctly capturing the effects of baroclinic instability, where eddy activity flattens isotherms (*a*) and thus cools the deep water and creates a sharper thermocline (*b*). POP-Leray correctly captures this same process, but to a lesser degree than POP-α, so we conclude that LANS-α performs better than Leray in modeling oceanic baroclinic instability. These POP-α and POP-Leray simulations were run using a filter of width nine.

A direct correspondence between a specific value of α and filter width is difficult to make, but the 9×9 filter produces results similar to $\alpha = 1.5\Delta x$ or $\alpha = 1.75\Delta x$. The filter smoothing tends to achieve better temperature statistics (compared to higher resolution POP) than the Helmholtz inversion (not shown, see [41]). A Green's function analysis of the discrete Helmholtz inversion shows that it has a larger domain of influence, but that its coefficients drop off more rapidly from the center than the filters' do [41]. So the Helmholtz inversion and filters are similar, but not identical, in both their smoothing effects and the resulting turbulence statistics.

People who are new to LANS-α often wonder why KE increases as the smoothing parameter (alpha or the filter width) is increased. In their experience with dissipative closures,

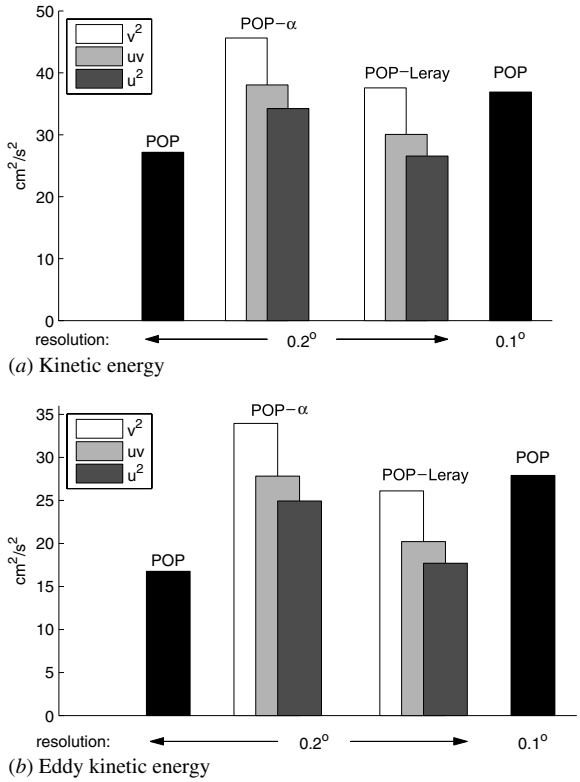

(*a*) Kinetic energy

(*b*) Eddy kinetic energy

Figure 7. Comparison of (*a*) kinetic energy and (*b*) eddy kinetic energy using three norms: u^2, uv and v^2 in the channel domain. This shows that POP-Leray is less energetic than POP-α when measured using the same norm. However, the conserved energy, which is uv for LANS-α and v^2 for Leray, is nearly equal. The POP-α and POP-Leray simulations were run with a filter of width nine.

simulations become less energetic as the smoothing parameter (e.g. the eddy viscosity) is increased. This reveals a fundamental difference between LANS-α/Leray and other turbulence models: LANS-α and Leray alter the nonlinear terms rather than the diffusive terms, and do not increase the dissipation. The smoothing operations are applied to the rough velocity **v** to obtain the smooth velocity **u**. LANS-α and Leray operate in such a way that a smoother advecting velocity allows the rough velocity to develop into a more energetic field. As **v** becomes more energetic, **u** becomes more energetic too (see figure 7). That is, because of the dynamics of the LANS-α parameterization, when **u** is much smoother than **v**, both velocities are more energetic than the velocity in a standard POP simulation.

A salient question about LANS-α is how it interacts with eddy viscosity turbulence models, and whether the two are compatible. Typical eddy viscosities in ocean models are orders of magnitude higher than the molecular viscosity of the real ocean to ensure numerical stability. POP-α must use an eddy viscosity model in conjunction with LANS-α, because LANS-α by itself does not provide a mechanism for energy dissipation near the gridscale. In fact, quite the opposite is true—LANS-α is more energetic than standard Navier–Stokes, and higher eddy viscosity coefficients are required to run stably at larger values of alpha. The data shown in figures 3–7 used biharmonic diffusion ($-\nabla^4$) with coefficients of

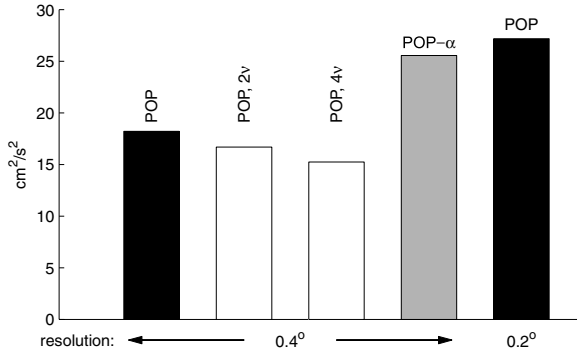

(*a*) Kinetic energy

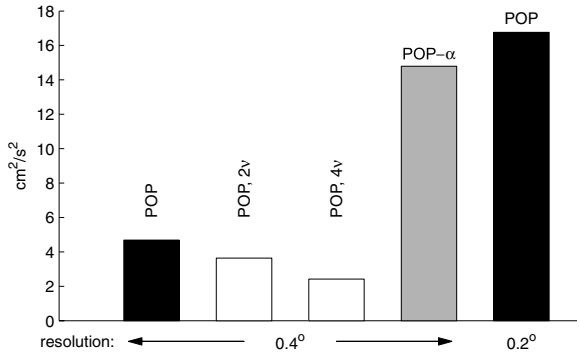

(*b*) Eddy kinetic energy

Figure 8. Comparison of (*a*) kinetic energy and (*b*) eddy kinetic energy using POP and POP-α, and from POP with a biharmonic diffusion coefficient that was doubled (2ν) and quadrupled (4ν). Higher viscous coefficients increase dissipation, reducing both measures. The LANS-α model is fundamentally different from diffusive turbulence closure schemes in that it increases, rather than suppresses, the eddy activity.

$6.9 \times 10^{12}, 8.6 \times 10^{11}, 1.1 \times 10^{11}$ and 1.4×10^{10} m^4 s^{-1} for resolutions of $0.8^\circ, 0.4^\circ, 0.2^\circ$ and 0.1°, respectively. We chose to keep the coefficient the same for all simulations at any one resolution so as to allow for unbiased comparison. One can increase viscosity in order to run POP-α stably at high values of alpha (e.g. simulations where alpha is greater than two gridcell widths). However, numerical stability constraints dictate that the timestep decreases at the same rate at which the eddy viscosity coefficient increases, so in practice running with large values of alpha and the associated higher viscosity is too expensive to be feasible as a turbulence model. In our experience to date, the best combination has been to use LANS-α with $\alpha = 1.5$–1.75 gridcell widths (or a nine-wide filter), in combination with biharmonic diffusion, using the standard POP diffusion coefficient for that resolution.

In order to show the effects of higher viscosity, simulations of POP using double and quadrupled values of the biharmonic viscosity coefficient (without LANS-α) were performed. Not only did the KE and EKE decrease, as expected, but the temperature profiles became worse (compared to higher resolution) as the coefficient increases and the action of eddies is suppressed. This exemplifies the key difference between LANS-α and the typical diffusive turbulence model: LANS-α actually allows more coherent structures to exist near the gridscale,

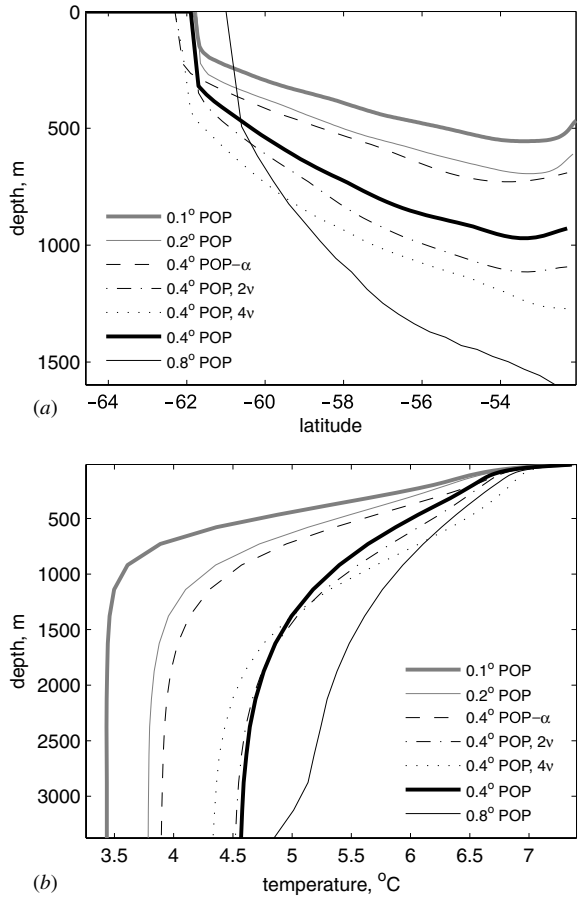

Figure 9. Comparison of equilibrium temperature distributions using POP and POP-α and from POP with a biharmonic diffusion coefficient that was doubled (2ν) and quadrupled (4ν). Descriptions are identical to figure 6. Increasing the viscous coefficient worsens the temperature profile, when compared to higher resolution POP data, whereas LANS-α increases eddy activity and is therefore able to improve the temperature structure through easing the onset of baroclinic instability.

while diffusive models damp out small-scale structure. This effect was predicted by earlier analytical work, as discussed in section 3: eddy viscosity models increase the forcing required to induce baroclinic instability, while for LANS-α the forcing required remains constant, and the critical wavenumber is lowered [33]. Lowering the critical wavenumber means that the physical processes of baroclinic instability, like eddy activity and flattening of isotherms, should occur in lower-resolution simulations. Indeed, this is exactly what occurs with POP-α (figures 3–7).

The Gent–McWilliams isopycnal tracer diffusion scheme discussed in section 2 is compatible with LANS-α. In preliminary simulations in the channel model domain, GM reduces KE and eddy activity but improves the temperature distribution in standard POP. Running GM in POP-α increases the KE and eddy activity over GM with standard POP. The combination of GM and POP-α requires a full parameter study, as one can vary diffusive

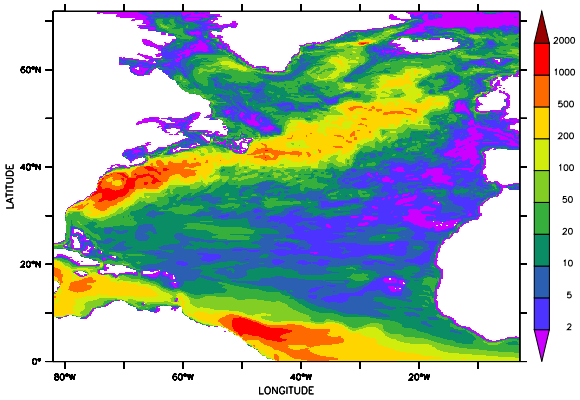

(*a*) POP, 0.2° resolution

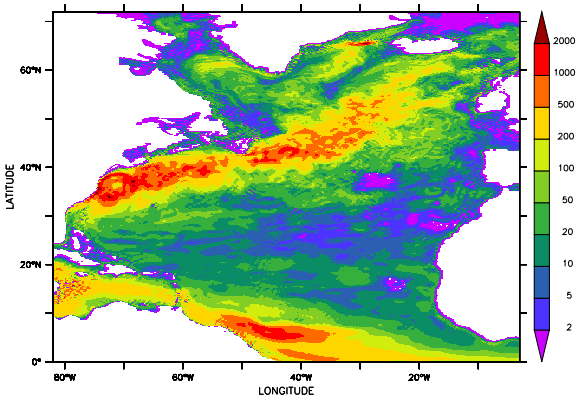

(*b*) POP-Leray, 0.2° resolution

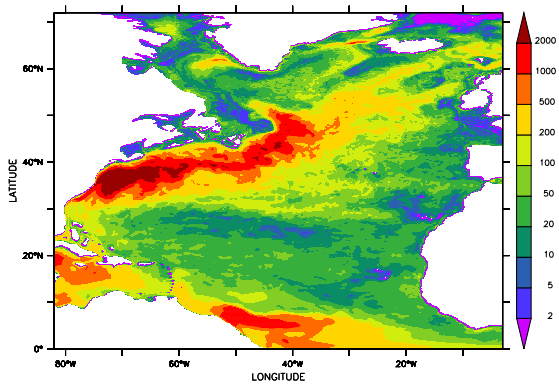

(*c*) POP, 0.1° resolution

Figure 10. Eddy kinetic energy in 0.2° North Atlantic simulations using (*a*) POP and (*b*) POP-Leray, averaged over 3 years and between 75 and 100 m depth, in $cm^2\ s^{-2}$, using the uv norm for POP-Leray. Pop-Leray has higher eddy kinetic energy in the North Atlantic Current, as can be seen by the stronger oranges and reds south of Greenland in (*b*), relative to (*a*). Panel (*c*) is from a better resolved 0.1° version of POP, from case 14b of [20], and is representative of the more realistic level of variability and pattern of mean circulation we would like to achieve.

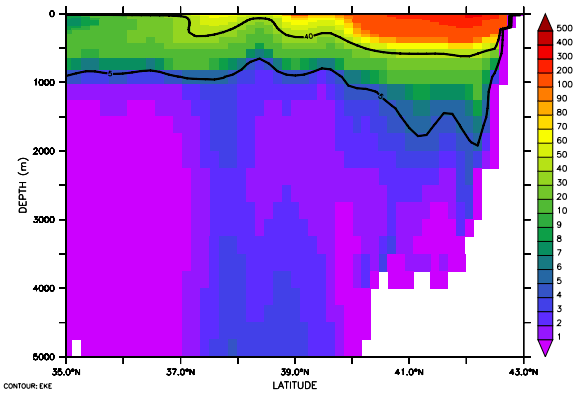

(*a*) POP, 0.2° resolution

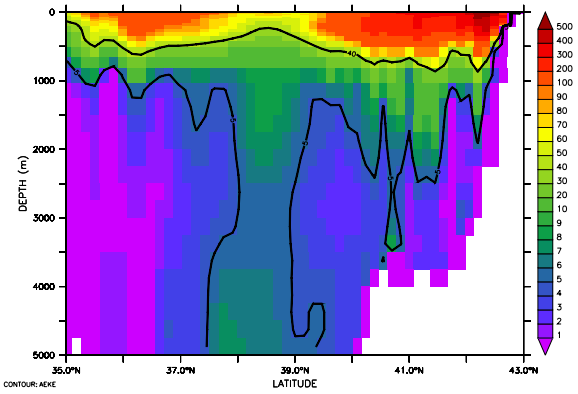

(*b*) POP-Leray, 0.2° resolution

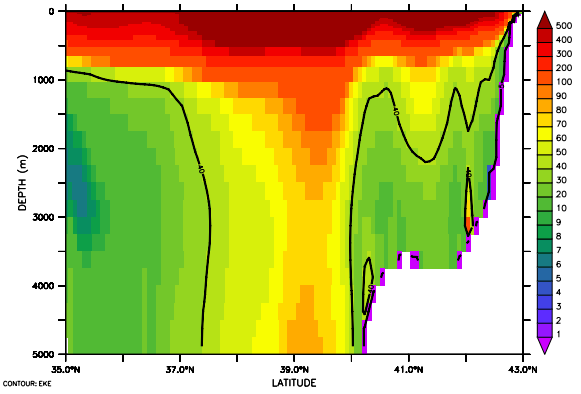

(*c*) POP, 0.1° resolution

Figure 11. Vertical section of eddy kinetic energy through the free jet of the Gulf Stream at 50° W using (*a*) 0.2° POP and (*b*) 0.2° POP-Leray, (*c*) 0.1° POP, in $cm^2\ s^{-2}$, using the uv norm for POP-Leray. Curves are contours of 5 and 40 $cm^2\ s^{-2}$. There is a deeper penetration of eddy kinetic energy using POP-Leray than POP.

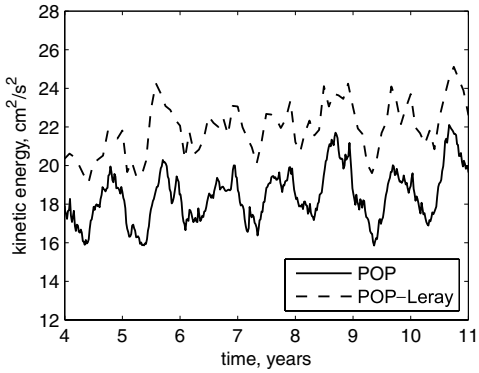

Figure 12. Kinetic energy, averaged over the domain, of POP and POP-Leray versus time for the 0.2° North Atlantic simulations. POP-Leray's kinetic energy (measured in the uv norm) is higher than POP. Higher kinetic energy is more realistic, as judged by higher resolution POP simulations (see table 1), and as inferred from satellite-based altimetry [14].

coefficients in GM as well as alpha (or filter width) in LANS-α. This will be the topic of a future paper.

After the idealized channel domain, we proceeded to a North Atlantic domain with 40 non-uniformly spaced vertical levels and 0.2° resolution, spanning from 20° S to 73° N, including the Gulf of Mexico and the Western Mediterranean. Temperature and salinity were restored to seasonal climatology in a 3° wide buffer along open boundaries, and the surface was driven by observed daily mean surface winds from 1985 to 2000 and monthly mean climatological heat fluxes (see [14, 20] for further details of this experiment design).

Experience with high-resolution North Atlantic simulations using standard POP shows that KE and EKE increase as resolution increases from 0.5° to 0.1°, and that model results at 0.1° agree well with observations of the magnitude and geographical distribution of EKE and sea-surface height variability [14, 20]. In particular, characteristics of the Gulf Stream become more realistic with higher resolution, including the location of Gulf Stream separation from the East Coast of the US at Cape Hatteras, the structure of the 'Northwest Corner' where the North Atlantic current turns north toward the Labrador Sea (figure 10(c)), the magnitude of EKE, and the depth-penetration of EKE in the free jet region of the Gulf Stream (figure 11(c)).

Our implementation of LANS-α for the North Atlantic domain is a work in progress, and is not yet complete. The rough topography, fast boundary currents and fuller spectrum of forcing make the North Atlantic more subject to instability than the idealized channel problem. Topics of inquiry include how to handle lateral boundary conditions with complex topography, whether to taper the smoothing parameter as one approaches the boundary (see [41], section 4), and whether to use depth-dependent smoothing in POP's split baroclinic/barotropic time-stepping scheme. Here we present results from Leray simulations in the North Atlantic domain using a filter of width nine and the same boundary methods as the channel domain simulations [41]. The Leray model is less energetic than LANS-α (figure 4), and has been shown to be more robust [40, 42], and so serves as an easier test-bed for these initial simulations.

POP-Leray ran stably in the North Atlantic domain for the duration of the simulation, over 10 years. Eddy kinetic energies of the Gulf Stream and North Atlantic Current are higher in POP-Leray than in POP, when the comparison is made at the same resolution of 0.2°

Table 1. Comparison of kinetic and eddy kinetic energy in the North Atlantic domain. Statistics for POP-Leray (using the uv norm) are higher than POP at the same resolution.

	POP, 0.2°	POP-Leray, 0.2°	POP, 0.1°
KE	17.3	22.1	42.6
EKE	11.1	13.1	29.4

(figure 10). Deeper penetration of eddy activity is also seen, as shown in a cross section through the free jet of the Gulf Stream (figure 11). Globally averaged statistics of KE and EKE also show a strong increase with resolution, and indicate again that POP-Leray produces higher energies than POP at the same resolution (figure 12 and table 1). The gains using POP-Leray are modest when compared to a doubling of resolution (also shown in these three figures and the table), but are consistent with POP-Leray results in the channel domain (figures 4 and 5), where the Leray model shows the same trends as LANS-α, but to a lesser degree. The Northwest Corner is not present in either the 0.2° POP or the 0.2° POP-Leray simulations, but is present in the 0.1° POP simulation (figure 10). A more realistic Northwest Corner and Gulf Stream separation will be an important measure of success for future POP-α simulations of the North Atlantic. The experiments described here demonstrate the technical feasibility of POP-Leray simulations in realistic oceanic domains with complex bathymetry.

6. Conclusion

We have shown that LANS-α can achieve eddy kinetic energy that is near to or greater than that of a doubled-resolution oceanic simulation without LANS-α. Temperature distributions also become more realistic as eddy activity increases, showing that LANS-α properly captures the physics of baroclinic instability. The Leray model improves turbulence statistics in the same manner as LANS-α, but to a lesser degree. The addition of either parameterization to POP adds about 30% to the computational time [41], so it is a small expense compared to an actual doubling of resolution, which increases computational time by a factor of 8–10. Implementation of LANS-α to accommodate the complex topography of the North Atlantic is not yet complete, but preliminary simulations with the Leray model show promising results: higher kinetic and eddy kinetic energy basin-wide, and deeper penetration of eddy kinetic energy in the free jet region of the Gulf Stream.

The success of LANS-α and Leray raises the question of *how* these parameterizations improve turbulence statistics. At current global ocean modeling resolutions of 1° to 0.2°, this is explained in part by the kinetic energy forcing scale, which is at or below the grid scale. Ocean-climate modeling is unique in computational fluids in that the forcing scale is unresolved. Using a linear stability analysis, we have shown that LANS-α (and Leray) shift the critical wavenumber to a lower wavenumber, allowing the conversion of baroclinic potential energy to barotropic kinetic energy, through baroclinic instability, to occur at a lower resolution than would otherwise occur. Numerical results show that this forcing occurs in a physically realistic way: tilted isopycnals are flattened, and eddy activity increases, as is observed in higher-resolution simulations.

Reducing the critical wavenumber of the kinetic energy forcing scale is only a partial answer to how LANS-α works. After all, many numerical studies using LANS-α have shown improved small-scale statistics in non-geophysical simulations where rotation is not present

[43, 44, 40]. Here the forcing is well resolved, but LANS-α still improves the simulation accuracy, when compared to experiments or high-resolution simulations. So LANS-α has potential use in regional or global ocean modeling at resolutions of 0.1° and higher, where the largest kinetic energy forcing scale is well resolved.

A possible criticism of the LANS-α model is that altering the kinetic energy forcing scale unrealistically changes the dynamics of the simulation compared to the real ocean. One must keep in mind, however, that other closure models change the forcing scale as well. We have shown that both Laplacian diffusion and hyperviscosity shift the critical wavenumber to a lower value [33]. Worse yet, they require a higher forcing to initiate instability, since both rely on diffusion to close the equations. LANS-α reduces the critical wavenumber, but does not increase the forcing required to trigger baroclinic instability. These comments apply equally to the Leray model.

LANS-α is fundamentally different from other turbulence closures in that it alters the nonlinear terms, rather than adding artificial diffusion in the viscous term. LANS-α accounts for the effects of the small scales on the large through nonlinear dispersion. This results in more energetic solutions, with more eddy structure near the grid scale.

LANS-α is primarily concerned with parameterizing the effects of horizontal mesoscale eddies. It does not replace parameterizations like KPP and Pacanowski and Philander, which account for mixing due to internal waves, vertical shear instability and convective instability, but may be run in conjunction with them. LANS-α may also be run with the Gent–McWilliams isopycnal tracer diffusion scheme, since they are implemented in the momentum and tracer equations, respectively. Future work will focus on how to optimally combine all of these parameterizations and implement LANS-α in global ocean simulations for climate change research.

Acknowledgments

This work was presented as a contribution to the conference at EPFL celebrating the 60th birthday of D D Holm. We would like to thank the organizers and scientific committee for this conference (R Camassa, M Hyman, J Marsden, T Ratiu and E Titi) for their exceptional care and thoughtfulness. We are also grateful to the Center Interfacultaire Bernoulli at EPFL for providing financial support for the conference, and to the staff of the Center for their cheerful and competent assistance at the conference. The work of DDH was also partially supported by the US Department of Energy, Office of Science, Applied Mathematical Research, and the Royal Society of London Wolfson Research Merit Award.

References

[1] Landau L D and Lifshitz E M 1971 *Physique théorique, vol 6: Mécanique des fluides* (Moscow, USSR: Editions MIR)
[2] Frisch U 1995 *Turbulence: The Legacy of A N Kolmogorov* (Cambridge: Cambridge University Press)
[3] Leray J 1934 Essai sur le mouvement d'un liquide visquex emplissant l'espace *Acta Math* **63** 193–248
[4] Gallavotti G 1993 Some rigorous results about the 3D Navier–Stokes equations *Les Houches 1992 NATO ASI Meeting on Turbulence in Extended Systems* (New York: Nova Science) pp 45–81
[5] Holm D D 1999 Fluctuation effects on 3D Lagrangian mean and Eulerian mean fluid motion *Physica* D **133** 215–69
[6] Large W G, McWilliams J C and Doney S C 1994 Oceanic vertical mixing: a review and a model with a nonlocal boundary layer parameterization *Rev. Geophys.* **32** 363–404
[7] Pacanowski R C and Philander S G H 1981 Parameterization of vertical mixing in numerical models of tropical oceans *J. Phys. Oceanogr.* **11** 1443–51

[8] Solomon H 1971 On the representation of isentropic mixing in ocean circulation models *J. Phys. Oceanogr.* **1** 233–4
[9] Redi M H 1982 Oceanic isopycnal mixing by coordinate rotation *J. Phys. Oceanogr.* **12** 1154–8
[10] Cox M 1987 Isopycnal diffusion in a z-coordinate ocean model *Ocean Modelling* **74** 1–5
[11] Gent P R and McWilliams J C 1990 Isopycnal mixing in ocean circulation models *J. Phys. Oceanogr.* **20** 150–5
[12] Boville B A and Gent P R 1998 The NCAR climate system model, version one *J. Clim.* **11** 1115–30
[13] Hallberg R and Gnanadesikan A 2006 The role of eddies in determining the structure and response of the wind-driven Southern Hemisphere overturning: results from the modeling eddies in the Southern Ocean (MESO) Project *J. Phys. Oceanogr.* **36** 2232–52
[14] Smith R D, Maltrud M E, Bryan F O and Hecht M W 2000 Numerical simulation of the North Atlantic Ocean at $1/10^o$ *J. Phys. Oceanogr.* **30** 1532–61
[15] Hurlburt H E and Hogan P J 2000 Impact of $1/8^\circ$ to $1/64^\circ$ resolution on Gulf Stream model–data comparisons in basin-scale subtropical Atlantic Ocean models *Dyn. Atmos. Ocean* **32** 283–329
[16] Maltrud M E and McClean J L 2005 An eddy resolving $1/10^\circ$ ocean simulation *Ocean Modelling* **8** 31–54
[17] Chassignet E P and Garraffo Z D 2001 Viscosity parameterization and Gulf Stream separation *Proc. 'Aha Huliko'a Hawaiian Winter Workshop* ed P Muller and D Henderson pp 367–74 (University of Hawaii)
[18] Smith R D and Gent P R 2004 Anisotropic GM parameterization for ocean models *J. Phys. Oceanogr.* **34** 2541–64
[19] Hecht M W, Hunke E, Maltrud M E, Petersen M R and Wingate B A 2008 Lateral mixing in the eddying regime and a new broad-ranging formulation *Ocean Modeling in an Eddying Regime (Geophysical Monograph Series)* ed M Hecht and H Hasumi (Washington, DC: American Geophysical Union)
[20] Bryan F O, Hecht M W and Smith R D 2007 Resolution convergence and sensitivity studies with North Atlantic circulation models: Part I. The western boundary current system *Ocean Modelling* **16** 141–59
[21] Sasaki H, Sasai Y, Nonaka M, Masumoto Y and Kawahara S 2006 An eddy-resolving simulation of the quasi-global ocean driven by satellite-observed wind field *J. Earth Simulator* **6** 35–49
[22] Smagorinsky J 1963 General circulation experiments with the primitive equations: i. The basic experiment *Mon. Weather Rev.* **91** 99–164
[23] Griffies S M and Hallberg R W 2000 Biharmonic friction with a Smagorinsky-like viscosity for use in large-scale eddy-permitting ocean models *Mon. Weather Rev.* **128** 2935–46
[24] McWilliams J C and Chow J H 1981 Equilibrium geostrophic turbulence: I. A reference solution in a beta-plane channel *J. Phys. Oceanogr.* **11** 921–49
[25] Salmon R 1980 Baroclinic instability and geostrophic turbulence *Geophys. Astrophys. Fluid Dyn.* **15** 167–211
[26] Salmon R 1998 *Geophysical Fluid Dynamics* (Oxford: Oxford University Press)
[27] Fu L L and Flierl G R 1980 Nonlinear energy and enstrophy transfers in a realistically stratified ocean *Dyn. Atmos. Oceans* **4** 219–46
[28] Hua B L and Haidvogel D B 1986 Numerical simulations of the vertical structure of quasi-geostrophic turbulence *J. Atmos. Sci.* **43** 2923–36
[29] Scott R B and Wang F 2005 Direct evidence of an oceanic inverse kinetic energy cascade from satellite altimetry *J. Phys. Oceanogr.* **35** 1650–66
[30] Scott R B and Arbic B K 2007 Spectral energy fluxes in geostrophic turbulence: implications for ocean energetics *J. Phys. Oceanogr.* **37** 673–88
[31] Karsten R, Jones H and Marshall J 2002 The role of eddy transfer in setting the stratification and transport of a circumpolar current *J. Phys. Oceanogr.* **32** 39–54
[32] Henning C C and Vallis G K 2005 The effects of mesoscale eddies on the stratification and transport of an ocean with a circumpolar channel *J. Phys. Oceanogr.* **35** 880–96
[33] Holm D D and Wingate B A 2005 Baroclinic instabilities of the two-layer quasigeostrophic alpha model *J. Phys. Oceanogr.* **35** 1287–96
[34] Holm D D, Jeffery C, Kurien S, Livescu D, Taylor M A and Wingate B A 2005 The LANS-alpha model for computing turbulence: origins, results, and open problems *Los Alamos Sci.* **29** 152–72 available at http://la-science.lanl.gov/lascience29.shtml
[35] Holm D D and Nadiga B T 2003 Modeling mesoscale turbulence in the barotropic double-gyre circulation *J. Phys. Oceanogr.* **33** 2355–65
[36] Hecht M W, Holm D D, Petersen M R and Wingate B A 2008 Implementation of the LANS-alpha turbulence model in a primitive equation ocean model *J. Comput. Phys.* **227** 5691–716
[37] Collins W D *et al* 2006 The community climate system model version 3 (CCSM3) *J. Clim.* **19** 2122–43
[38] Meehl G A *et al* 2006 Climate change projections for the twenty-first century and climate change commitment in the CCSM3 *J. Clim.* **19** 2597–616

[39] IPCC 2007 *Climate Change 2007: The Physical Science Basis. Contribution of Working Group I to the Fourth Assessment Report of the Intergovernmental Panel on Climate Change* (Cambridge University Press)
[40] Geurts B J and Holm D D 2002 Alpha-modeling strategy for LES of turbulent mixing *Turbulent Flow Computation* (Dordrecht: Kluwer) chapter 7, pp 237–78
[41] Petersen M R, Hecht M W and Wingate B A 2008 Efficient form of the LANS-alpha turbulence model in a primitive-equation ocean model *J. Comput. Phys.* **227** 5717–35
[42] Geurts B J and Holm D D 2006 Leray and LANS-α modeling of turbulent mixing *J. Turbul.* **7** 10
[43] Chen S, Foias C, Holm D D, Olson E, Titi E S and Wynne S 1999 The Camassa–Holm equations and turbulence *Physica* D **133** 49–65
[44] Chen S, Holm D D, Margolin L G and Zhang R 1999 Direct numerical simulations of the Navier–Stokes alpha model *Physica* D **133** 66–83
[45] Wingate B A 2004 The maximum allowable time step for the shallow water alpha model and its relation to time-implicit differencing *Mon. Weather Rev.* **132** 2719–31